Proceedings World Geothermal Congress 2015
Melbourne, Australia, 19-25 April 2015

3D Natural State Model of the Menengai Geothermal System, Kenya

Montegrossi G.[1], Pasqua C.[2], Battistelli A.[3], Mwawongo G. [4], Ofwona C.[4]

[1]CNR – IGG, Firenze, Italy, [2]ELC Electroconsult SpA, Baranzate (MI), Italy,

[3]Saipem SpA, Fano (PU), Italy, [4]GDC, Nairobi, Kenya

montegrossi@igg.cnr.it, claudio.pasqua@elc-electroconsult.com, alfredo.battistelli@saipem.com, gmwawongo@gdc.co.ke, cofwona@gdc.co.ke

Keywords: Rift Valley, conceptual model, numerical simulation, Petrasim, TOUGH2

ABSTRACT

The Menengai caldera is an elliptical depression with minor and major axes measuring about 8 and 12 km respectively, located near Nakuru, Kenya's Rift Valley. Geophysical investigations (micro-seismic monitoring, gravity and MT surveys), geological surveys, geochemical surveys (fumaroles sampling, soil gas surveys) and a soil temperature survey allowed Geothermal Development Company (GDC) to locate the first exploratory well MW-01 which intercepted a deep reservoir with temperatures exceeding 300°C, found beneath a shallower liquid-dominated reservoir at a temperature in the range 190-200°C. The exploratory and development drilling campaign, which is undergoing, provided the drilling of some 20 deep wells by December 2013 aimed at characterizing the deep reservoir properties, delineate the field extension and provide additional steam for power development. The geochemical data acquired with production well testing allowed not only to characterize the chemistry of the shallow aquifer and of the deep steam-dominated reservoir, but indicates also an 'intermediate temperature zone' that could be interpreted as a 'rim' of the deep reservoir. Surface exploration surveys and the findings derived from drilling, logging and testing of geothermal wells were used to build a 3D numerical model of the geothermal system natural state by means of the TOUGH2 reservoir simulator, supported by Petrasim 5.3 graphical interface. The numerical model was intended to check the consistency of the conceptual model, give a better picture of the reservoir thermodynamic conditions, and constrain the mass and heat flows through the system. Making in numbers the idea arisen in the conceptual model, the 3D natural state has been reconstructed by simulating the heating up due to a hot intrusion in a complex system. The complexity of the system arises in a particular structure consisting in a deep vapor-dominated high temperature reservoir just on top of the hot intrusion at temperatures higher than 300°C, separated from the shallower liquid-dominated reservoir (with temperatures ranging from 130 up to 210°C) by a relatively thin impermeable layer. The model was run to steady-state conditions, and calibrated against data obtained from geochemical investigations, well pressure and temperature profiles recorded under warm-up and flowing conditions, as well as available production test results. The details about the 3D model construction within TOUGH2 and Petrasim and the results of the simulated natural state are presented and discussed.

1. INTRODUCTION

Geothermal development along the African Rift is a scientific challenge whose main target is to find an energy supply with low environmental impact for many growing economies. The challenge nowadays is no longer limited to find the three key points needed for a geothermal reservoir to exist (i.e. temperature, permeability and fluids) but also to provide a sounding basis for the evaluation of the economic performance of the geothermal prospect. The numerical model is the main tool for synthetizing all the geological, geophysical, geochemical and reservoir engineering findings, under the guidance of a conceptual model.

The Menengai geothermal prospect is located on the outskirts of Nakuru town, situated about 180km west of Nairobi, and covers an area of about 110km^2. Most of the area is well served by a network of earth roads and all weather roads.

The geothermal field has been the object of geoscientific investigations since the sixties, while underground exploration started in February 2011 through drilling of deep wells. Since that time until the end of December 2013 20 wells have been drilled (out of which three were abandoned before reaching their final depth) and additional wells are being drilled.

2. CHARACTERIZATIONOF MENENGAI GEOTHERMAL SYSTEM

2.1Geoscientific Investigations

2.1.1 Geology

The most significant geological findings are summarized hereafter:

- The main heat source of the geothermal system is presumed to correspond to the magmatic chamber responsible for the emission of the huge volume of pyroclastic flows that brought about the formation of the Menengai caldera.
- The occurrence of very recent volcanic products (lavas and tuffs) within the caldera indicates that such chamber is still active and its top is found at a very shallow depth, presumably in the 5 to 10km range. Based on the temperatures registered in the wells (see Figures 3 and 5), the most shallow portion of the magmatic chamber is situated in the western part of the caldera, in correspondence of wells MW-04 and MW-06.
- The formations outcropping within the caldera and those intersected by the wells are of peralkaline trachytic composition, presumably derived from fractionation of basaltic magmas, and consist predominantly of lavas, with subordinate pyroclastic intercalations and with a progressive increase of intrusive products towards the wells bottom and in the central portion of the investigated sector.

- The structure at a regional level is controlled by the family of N-S faults of tensional type, which extend along the Rift and constitute the main Tectono-Volcanic Axes (TVA) recognized in the area, that is the Molo and Solai systems presumed to form a complex graben & horst system. However, within the Menengai caldera other fault systems become predominant, in particular the NNW-SSE structures, which are highlighted by the occurrence of well aligned eruption centres and fumarolic activity. Another important system corresponds to the E-W direction expressed by a long-liner extending between MW-01 and MW-03 and by other parallel faults, which seem to partly control the areal extent of the reservoir.

- Two structures of the NNW-SSE system (trending N.7W and N.30W) appear to be of major importance, as indicated by their pronounced surface expression, their control over the volcanic emission centres and the association with high intensity of the linear features. These structures, also clearly expressed by the distribution of the micro-seismic events, define a block of 4 to 6km wide, which extends throughout the caldera and where all the deep wells drilled to date are located, except MW-07, which falls at the western margin of this block.

- As refers to secondary mineralogy, it is observed that the minerals indicative of high formation temperature, that is quartz, pyrite and epidote, appear in general at an average depth of 600-800m, corresponding to an approximate elevation of 1400 m.a.s.l. The only exceptions to this refer to wells MW-05A and partly MW-07, 08 and 12, where the high temperature minerals, which characterize the propylitic zone, are found below elevation 1000 m.a.s.l.

- A pronounced dome-like shape of the top of the propylitic zone, as expressed by the first appearance of epidote, has been recognized, being the upper portion in correspondence of a W-E oriented belt which extends between MW-07 and MW-03. Such configuration might reflect the location of the main upflow sector of the geothermal system.

- From the stratigraphic point of view, no specific geological units can be singled out as playing the role of cap-rock or reservoir. In fact, the whole stratigraphic sequence consists predominantly of trachytic lava, wherefore its permeability conditions depend essentially on the type and degree of hydrothermal alteration and on the extent and age of tectonic activity.

- From the structural point of view (Figure 1), an intense neo-tectonic activity has taken place within the Menengai caldera, as expressed by the high density of the linear features. The above mentioned structural block delimited by the N.7W and N.30W faults is deemed to control the lateral extent of the geothermal system and to host the most shallow and active portion of the magmatic chamber.

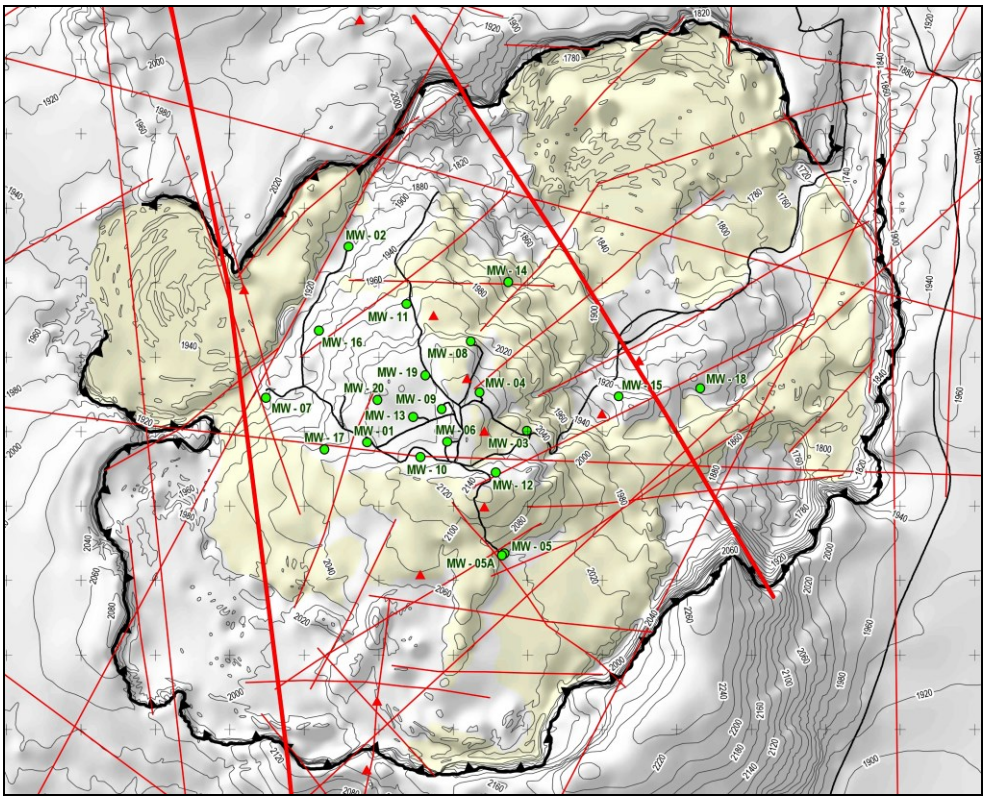


Figure 1: Structural scheme of the Menengai caldera and wells location.

2.1.2 Geophysics

The geophysical dataset available for the Menengai caldera and surrounding area includes the following:

a. Gravity stations fairly regularly distributed throughout the Menengai caldera and in the northern region.

b. 80 Time-Domain Electro-Magnetics (TDEM) stations and some 100 Magnetotelluric (MT) stations distributed in an irregular way within the Menengai caldera.

The analysis of gravity data puts into evidence a well-pronounced positive anomaly in correspondence of the Menengai caldera, which extends to the north encompassing the Ol Rongai sector to the NNW. The anomaly can be modeled with a body, below the caldera, with a density of 2,900kg m^{-3} enclosed in a surrounding medium of about 2,740kg m^{-3}. The high-density body below the Menengai caldera could be interpreted as belonging to a magma chamber, although it is deemed that such interpretation should be further evaluated. In fact, recent literature suggests that the northward continuation of the gravity high in the Ol Rongai sector is due to a gabbroic intrusion associated with differentiation of a mafic (basaltic) magma. The presence of a less acidic and therefore denser magma chamber beneath the caldera area and its surroundings, where generally a sequence of trachytic lavas crops out, is compatible with a possible path of magma differentiation. However, a density increase could be also related to secondary factors, such as the occurrence of high temperature hydrothermal alteration.

With reference to the electro-magnetic investigation, inversion of MT data generally showed that four electrostratigraphic units can be recognized:

- An uppermost resistive unit, with a thickness of 100-300m and a resistivity of 50-100Ωm;
- An underlying upper conductive unit, with an average thickness of 600-800m; and a resistivity usually ranging between 2 and 15Ωm;
- A resistive basement with a resistivity in of the order of 100Ω m, whose top may correspond to the top of the geothermal reservoir;
- A deep conductive unit, whose top is normally at a depth of around 10km. Only in a few soundings, located around the major NNW-SSE fault in the eastern part of the caldera, the top of the conductive unit occurs at a depth in excess of 15km. This unit has an average resistivity value of 5Ωm and could be related to deeper magmatism (underplating).

Finally, the micro-seismic monitoring (Simiyu, 2009) conducted over a zone of about 600km^2 mainly centered around the Menengai caldera provided very consistent results, by identifying the presence of three anomalies all characterized by a concentration of seismic events, shallow depth of the events themselves and low value of the V_p/V_s ratio, pointing to specific sectors with neo-tectonic activity and shallow depth of high temperature bodies. Two of the above anomalies occur in correspondence of the Molo and Solai TVA. The third and major one, under vapor dominated conditions, extends in the central portion of the Menengai caldera, encompassing a SW zone not yet tested by deep drilling.

2.1.3 Geochemistry

All the available geochemical data coming from deep geothermal wells (MW-01, 03, 04, 06, 09, 12 and 13), surface manifestations, shallow aquifers and soil gases have been reviewed with the aim to reconstruct the geochemical model of the Menengai prospect. The main results of the review are summarized hereafter.On the basis of available geochemical data, the geothermal reservoir present at depth inside the Menengai caldera comprises (see Figure 2):

(i) A shallow liquid dominated reservoir, at temperatures of 150-190°C, as suggested by water geothermometers, crossed by the wells MW-01, MW-03, MW-04, MW-12.

(ii) An intermediate reservoir, also crossed by a few wells, where inferred temperatures based on water geothermometers are 250-270°C for wells MW-01, MW-04, and MW-12, but 230°C only for well MW-03. It is possible that this intermediate reservoir could be hydraulically connected with the deep one, at least in the sectors of wells MW-01, MW-04, and MW-12.

(iii) A comparatively deep reservoir, at temperatures from 280 to >340°C, hosting fluids at different vapor/(vapor+liquid) mass ratios, y, as indicated by gas equilibria in the H_2O-CO_2-CH_4-H_2 system. In particular: (a) the central wells MW-06, MW-09, and MW-13, discharging superheated steam, as well as borehole MW-12 are connected with a deep vapor-dominated zone, where y is close to 1; (b) wells MW-04 and MW-01 (after the workover) intersect a deep two-phase zone where y is in the range 0.1 to 0.5; (c) wells MW-03 and well MW-01 (before the workover) seems to be in connection with a liquid-dominated deep zone, where y is close to 0. Well MW-01 has a very peculiar behavior since its deepest section has been connected with two deep feed zones with distinct vapor/(vapor+liquid) mass ratios. This fact is highlighted in the schematic cross-section of Figure 2 by the position of the well on the limit between the y~0 and the y~0.1-0.5 zones.

Irrespective of the provenance from the shallow or intermediate aquifer, all reservoir liquids belong to the Na-HCO_3 facies as Na (2,440 to 3,510 mg/kg) and total ionic carbonates (4790 to 8410mg HCO_3/kg, with $HCO_3^- >> CO_3^{2-}$) largely prevail over other cationic constituents (K from 74 to 220mg/kg, Ca from 0.1 to 0.9mg/kg, and Mg from 0.04 to 2.4mg/kg) and anionic ones. Average total dissolved solids range from 9,180 to 13,200mg/kg, while pH values, calculated through a mineral-solution equilibrium model, vary from 6.7 to 7.5.

With reference to gas geochemistry, it is observed that gas equilibrium temperatures of fluids from wells MW-01, MW-04, MW-09, MW-12, and MW-13 are generally > 340°C, whereas lower equilibrium temperatures are indicated by fluids from wells MW-03 (280-300°C) and MW-06 (from 280 to >340°C). These equilibrium temperatures are similar to or somewhat higher than those measured in the deepest portions of Menengai wells, suggesting that gases are chiefly contributed by the deepest high-temperature zones of the geothermal reservoir.

The analysis of the gas equilibrium suggests that there is an increase in y, that is in vapor/(vapor + liquid) mass ratio, moving not only towards the central zone (where the vapor-discharging wells MW-06, MW-09, and MW-13 are located), but also at greater depths.

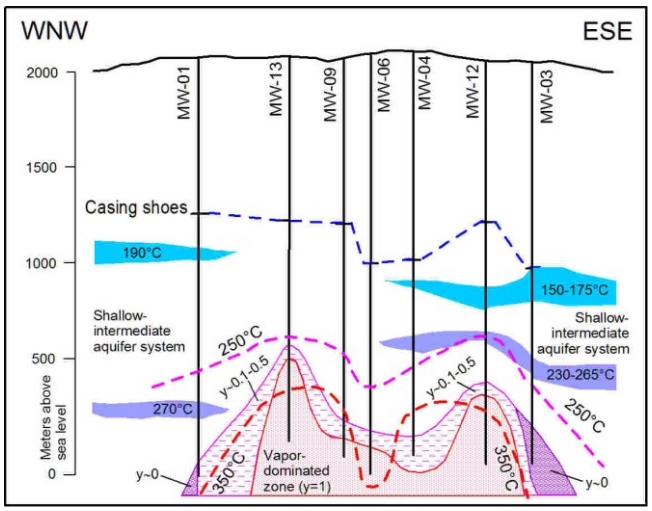


Figure 2: Schematic cross-section through the central area of the Menengai caldera showing the geothermal reservoirs encountered by the deep boreholes MW-01, MW-03, MW-04, MW-06, MW-09, MW-12, and MW-13.

2.2 Reservoir Engineering and Well Production

The reservoir engineering evaluation was performed by reviewing the data collected during drilling and testing of 16 wells completed at the date this study was finalized, while 4 additional wells were abandoned because of drilling problems (MW-05, 10, 14 and 18). Available data consisted in wells stratigraphy and completion, record of partial and total circulation losses; completion tests on 3 wells (MW-01, 02 and 19: water loss, step rate injection and falloff); pressure and temperature (P&T) surveys collected at well completion, during warm-up and production testing; spinner surveys on 3 wells (MW-02, 16 and 17); production tests on 7 wells (MW-01, 03, 04, 06, 09, 12, 13); composition of discharged fluids. Measurements performance in Menengai wells and data interpretation are complicate due to the challenging conditions encountered: extremely high temperatures, often above 300°C and reaching supercritical values up to 390°C at bottom hole; presence of multiple feed zones over extended wellbore sections at rather different thermodynamic conditions which are promoting important interzonal flows affecting both the recording of stabilized wellbore conditions and the well performance under production; presence of downhole scaling phenomena during production of some wells discharging two-phase fluids; contemporaneous operation of 4 drilling rigs requiring strong efforts in terms of personnel and equipment availability to implement all the necessary measurement and testing activities.

2.2.1 Reservoir Engineering

Few P&T logs and temperature build-ups were ran during drilling to minimize the associated risks. P&T logs were recorded during warm-up on all wells, while water loss tests and step rate injectivity tests were performed in 3 wells only (MW-01, 02, 19). P&T logs under flowing conditions were recorded in 4 wells (MW-01, 04, 12 and 13). Downhole logs were mostly ran using conventional mechanical instruments with calibration curves available up to 300°C. As in several wells the downhole temperature exceeds 300°C, reaching a maximum of 392°C recorded in well MW-04, the correction of pressure deflections for temperature effects above 300°C was not always reliable.

Most of the wells encountered a liquid dominated shallow reservoir with temperatures ranging from 130 to 210°C depending on well location distance with respect to the central area in correspondence of wells MW-06, 09 and 13, were the shallow reservoir was of reduced thickness or almost absent. Thanks to the wellbore cooling during drilling operations and cold water circulation losses encountered, most of the wells exhibited a column of liquid water during the initial warm-up. Wells drilled in the hottest area experienced a faster warm-up with the evolution of boiling conditions downhole (MW-06, 08, 09, 12, 13). Figure 3 shows the P&T logs recorded in well MW-08 after 3 months of warming-up: boiling conditions are present from about 1200 m to 1900 m depth along a column of liquid water. Other wells, generally located at the boundary of the present well field and crossing both the shallow and deep reservoirs, developed strong interzonal flows from upper cold liquid-dominated feeds towards the deep ones, preventing the warm-up of the latter (well MW-01, 02, 05A, 16 and 17). A good example of interzonal flows is given by well MW-05A drilled to the S of the developed area. Figure 4 shows the progressive warm-up with an almost vertical T profile between 1000 m and bottom hole at 2080 m. Liquid conditions prevail everywhere downhole with a pressure pivot point of 62 bara at a depth of 1200 m.

Useful indications about the pressure distribution with depth in the central developed area can be obtained looking at Figure 5 (left) showing the pressure profiles recorded in well MW-01 during drilling and warm-up. Log P1 was recorded in the 17 ½" open hole (OH); logs P4 and P5 in the 12 ¼" OH; logs P6 and P9 were recorded during the initial warm-up, while logs P24 and P25 were obtained after the workover performed to remove the obstruction found at 1780 m depth. During drilling of 17 ½" OH the static level was at about 1965 m.a.s.l., while it fall down to 1675 m.a.s.l. in the subsequent section, indicating a hydraulic barrier between 1700 and 1600 m.a.s.l. which separates ground water circulation from deeper thermal aquifers. During the initial well warm-up after the final depth was reached, the static level was approximately the same as in the section above with a pivot point at about 1100 m.a.s.l. This suggests that the pressure was controlled by upper liquid-dominated feeds belonging to the shallow reservoir which are locally close to hydrostatic equilibrium with colder thermal aquifers above. Logs P24 and P25 were ran during the warm-up after the well workover performed to remove an obstruction found at approximately 1780 m depth during a long term production test conducted in 2011.

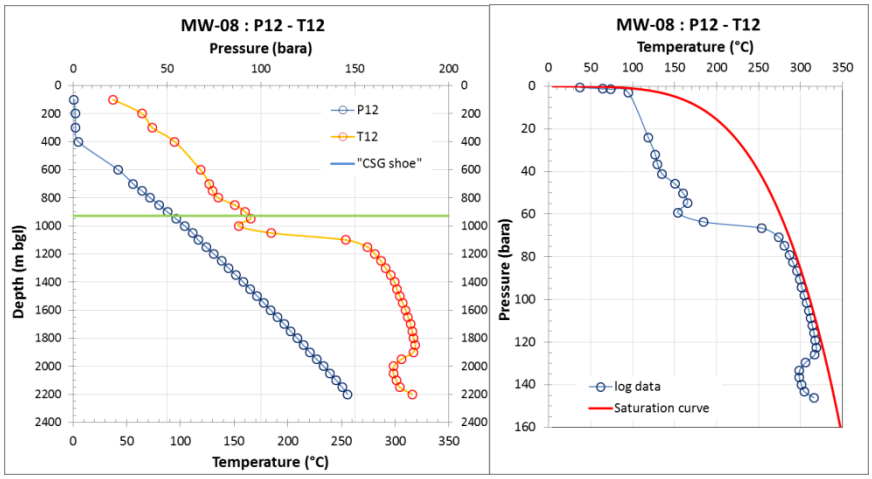


Figure 3: Temperature & pressure logs (left) and P&T measurements against the pure water saturation line (right) recorded in well MW-08 after 3 months of warm up.

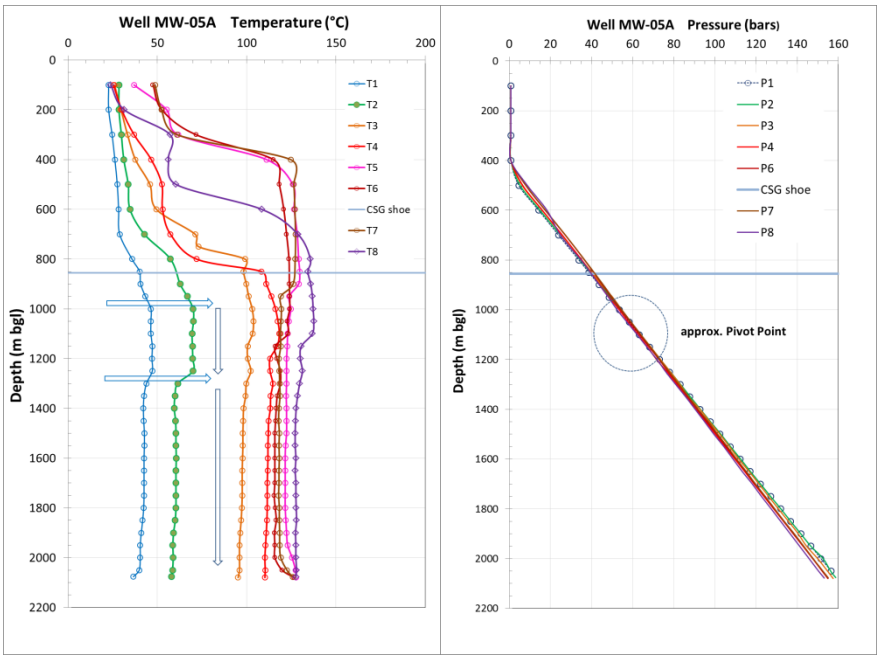


Figure 4: Temperature (left) and pressure (right) profiles recorded in well MW-05A during the warming up from March 26 to June 6, 2013.

These two logs show a completely different pressure distribution now dominated by deep feeds whose temperature exceeds 310°C. Figure 5 (center) presents the analysis of pressure gradients and fluid composition when logs P24 and T24 were ran. A column of two-phase fluid is present at elevations of 1330 – 330 m.a.s.l., between two sections with gas static pressure gradient. The two-phase section is likely to be supported by a boiling column of fluid with an interzonal flow from deep feeds at about 400 m.a.s.l. to the upper shallow reservoir feeds at 1050 m.a.s.l. Boiling promotes the exsolution of NCG (non-condensable gases) which accumulates in the colder upper well section, as clearly shown by the PT plot in Figure 5 (right). NCG content in boiling fluids is supporting the two-phase conditions with high local partial pressures which can be estimated in 20 to 40 bar. These NCG pressure do not reflect the actual NCG reservoir content, which is much smaller, but are due to the accumulation of NCG within the wellbore because of boiling. The lower gas section contains saturated steam (SS) and superheated steam (SH) at 371.7°C, close to the critical temperature of water. This lower section at bottom hole is likely to be controlled by the extremely high temperature present in an impervious basement where heat conduction predominates.

Logging and testing results prove that the shallow reservoir has a negative effect on both, wellbore evolution during warm-up, with interzonal flows preventing the heating of deep well section due to the continuous down flow of cold brine, and on production capabilities. In fact, despite of a possible increment of total mass discharge, the mixture enthalpy is reduced and this has also an impact on the flowing well head pressure (WHP). Well MW-01 represents an exception to this general behavior, with about 80% of total mass coming from the shallow reservoir as estimated from geochemical data processing and heat and mass balance calculations. But the steam supplied by shallow reservoir feeds amounts at separation pressure to less than 30% of total steam production. The above considerations suggest to complete future wells by avoiding the negative effects of shallow reservoir feeds. Running of deeper production casing (CSG) shoes is deemed necessary and should be decided on a well by well basis as function of encountered local conditions which need to be carefully evaluated during well drilling.

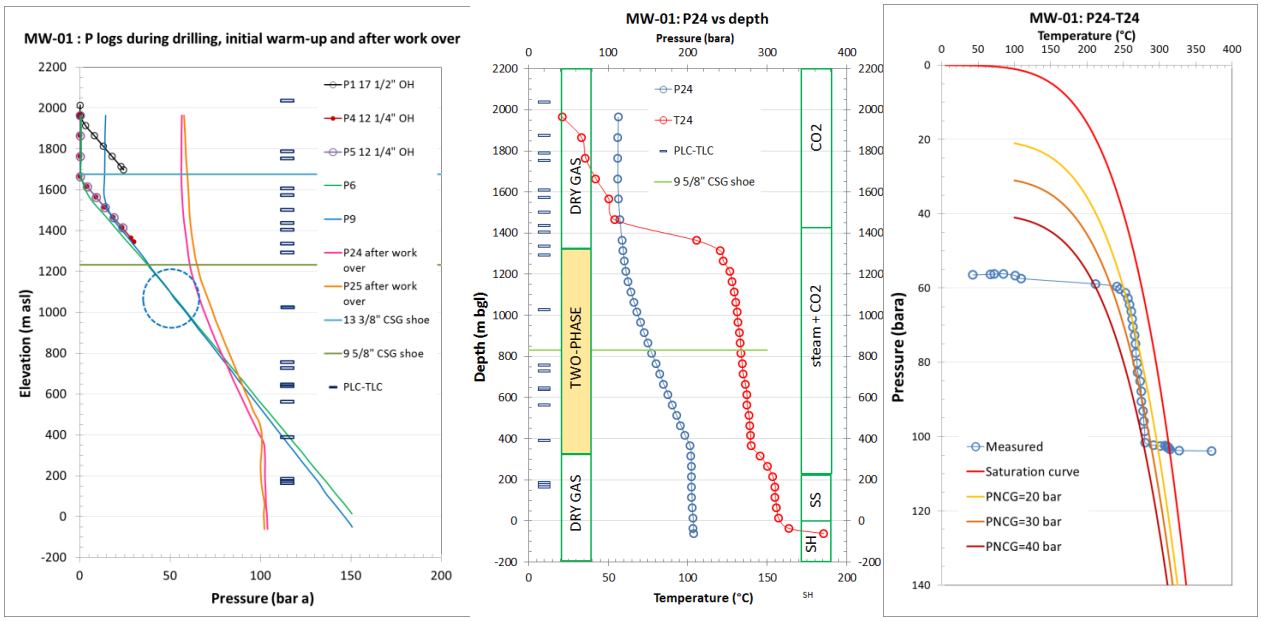


Figure 5: Pressure logs recorded during drilling and warm-up (left). P24-T24 logs recorded after the work-over (center), and P24-T24 logs plotted on the PT space against the water saturation curve and boiling curves of mixtures of water and CO_2 at fixed partial pressure (right).

The evaluation of hydraulic parameters of deep reservoir was attempted by using the pressure transients recorded during step-rate injection tests and subsequent fall-off. Figure 6 shows the step-rate injection test recorded at 1800 m in well MW-01 and the evaluation of the Injectivity Index (II). Due to the presence of permeable zones below the instrument setting depth, cold water was also flowing beneath the P&T tools as clearly shown by the temperature reduction during injection from 180°C down to 55°C, with effects on recorded flowing pressure. Figure 7 shows the P&T recorded during the fall-off and the semi-log plot of pressure vs time for the evaluation of hydraulic transmissivity. After about 4 hours from injection shut-in the temperature shows a sudden increment which corresponds to a stabilization of pressure, suggesting that interzonal flows are likely to affect the pressure transient. The drawdown regression line was then evaluated using data recorded in the first 4 hours. The overall kh product is estimated in 12.3 Dm with a skin factor of -5. The II, kh product and skin factor estimated for wells MW-02 and MW-19 were 270 and 150 LPM/bar, 7.6 and 1.9 Dm, -4.4 and -5.5, respectively. An additional estimation of reservoir hydraulic parameters was attempted by using the pressure drawdown recorded downhole when running the P&T surveys under flowing conditions. Considering the data available and the variable pressure drawdown estimated at different depths, computed values were of limited reliability. No pressure transients were recorded during the production tests.

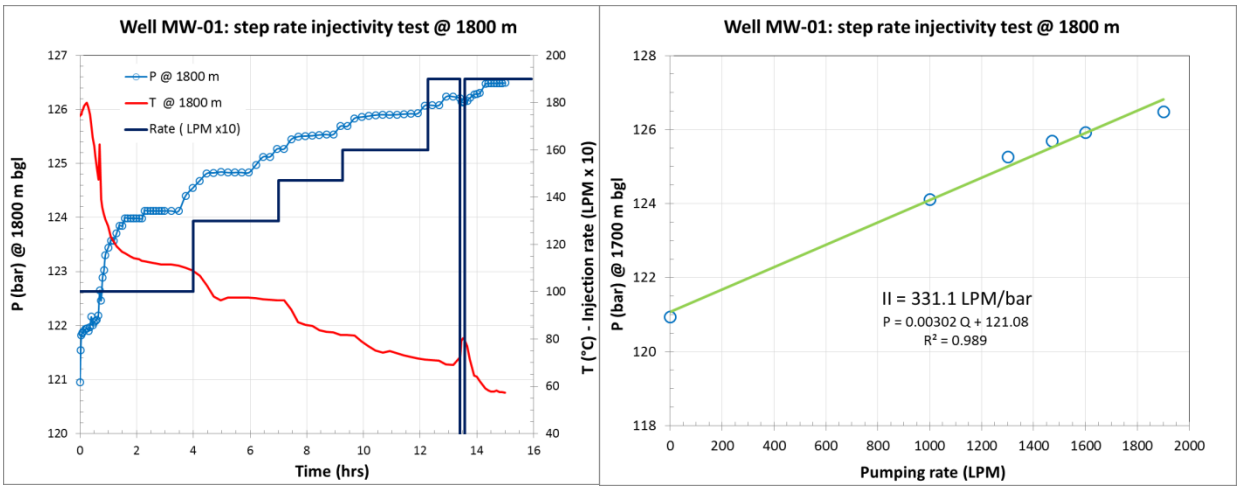


Figure 6: P&T at 1800 m depth and injection rate history during the step rate injection test performed in well MW-01 (left) and bottom hole P vs rate for the evaluation of II (right).

2.2.2 Well production features

Production tests were performed on 7 wells, out of which one, well MW-03, is a marginal two-phase producer discharging low enthalpy fluids from the shallow reservoir. Production tests were conducted using horizontal lines equipped with a lip pipe and discharging into one or two vertical twin-pipe atmospheric pressure separators (silencers). Brine rate was measured using sharp edged weir boxes. Total rate and enthalpy for two-phase discharge were computed using the R. James' approach by combining the

lip pressure and the weir box level readings (James, 1962; 1970). Dry steam discharge rates were computed using lip pressure readings and the enthalpy estimated at local thermodynamic conditions.

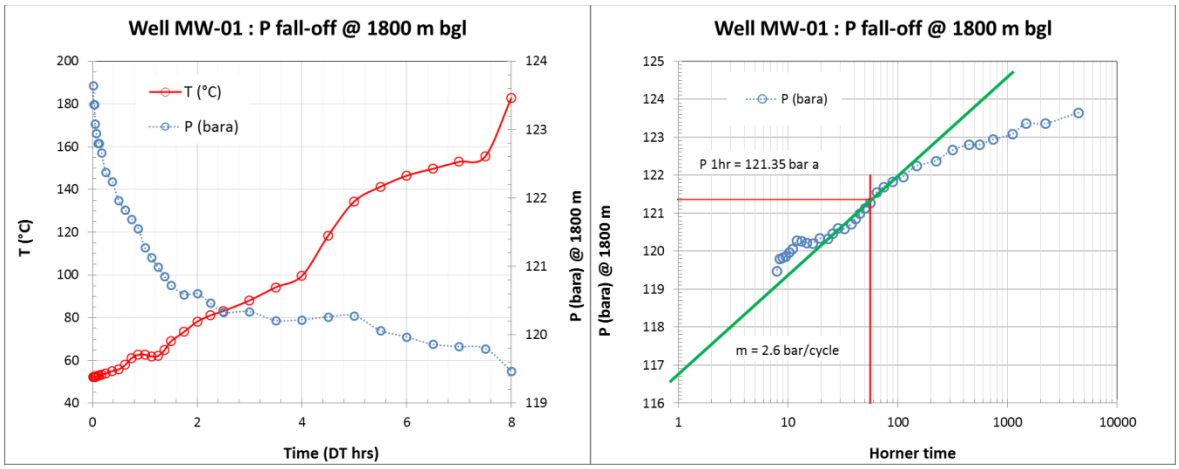


Figure 7: P&T at 1800 m depth recorded during the fall-off in well MW-01 (left) and the semilog plot of P vs Horner time for the evaluation of hydraulic transmissivity (right).

Production enthalpy depends strongly on the contribution of low temperature shallow reservoir. When this contribution is remarkable, as in wells MW-01, 04 and 12, two-phase discharge is present with enthalpies ranging from 1200 up to 1600 kJ/kg. Wells MW-06, 09 and 13, all located in the middle of field developed area, are characterized by dry steam discharge after few days of initial two-phase production. Two-phase wells MW-01 and MW-04 were characterized by the decline of discharge potential linked to scaling phenomena downhole, clearly detected by obstructions found at depths of 1790 and 1560 m, respectively. Workover operations conducted in well MW-01 were able to restore well production at rates, enthalpies and WHP even higher than those recorded at well start-up. An obstruction was also detected after only two-weeks in well MW-12 at a depth of 1588 m, after an important initial rate decline. Well MW-06 was also showing a remarkable production decline which is likely to be due to a combination of low reservoir permeability and scaling phenomena downhole. When production through 5" lip pipe started, a cycling discharge was recorded with sharp changes of WHP and total rate. Spot two-phase discharge was recorded during WHP surges, further indicating that cycling was probably linked to competing effects among multiple feeds with high enthalpy contrast. Cycling was followed by two-phase discharge. A few days later, a rather fast drop of WHP was recorded, partially recovered reducing the rate with 4" lip pipe. The relatively high CO_2 partial pressure and the processing of geochemical data with calculation of fluid chemical equilibrium suggest that the scaling is due to calcium carbonate precipitation.

The output curve in terms of mass rate and enthalpy vs WHP is shown for the two-phase wells MW-01 and MW-04 in Figure 8, and for the dry steam wells MW-09 and MW-13 in Figure 9. Both two-phase wells show the decline of discharge rate in time which is interpreted as the result of scaling downhole. Both wells show the dependency of enthalpy with WHP, with higher enthalpies recorded at high WHP (and low rates), in particular for well MW-04. This can be interpreted as the result of a lower contribution from the shallow reservoir when higher flowing pressures are present downhole.

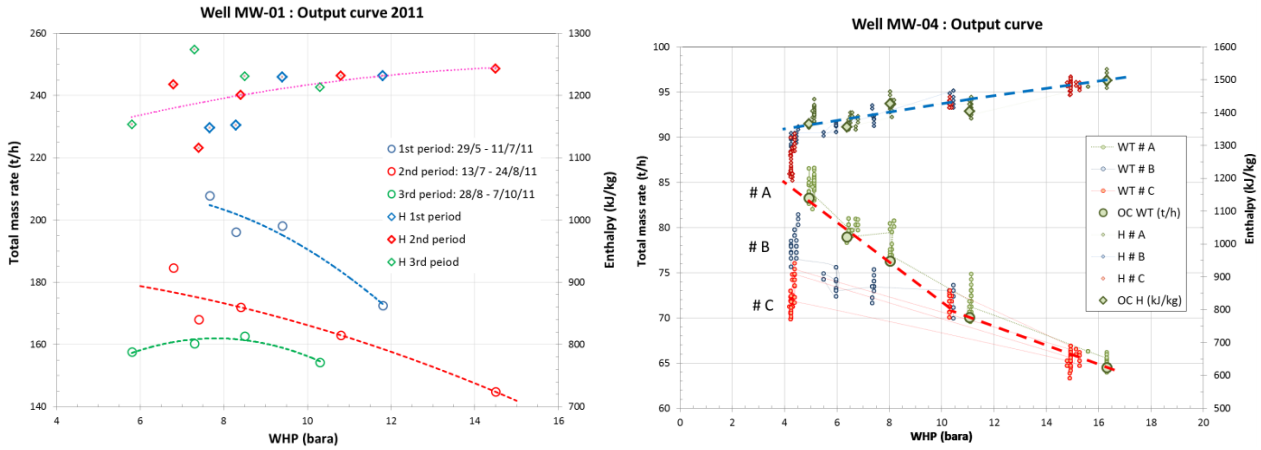


Figure 8: Output curves of wells MW-01 (production test in 2011) and MW-04 (three subsequent steps #A, #B and #C). Both wells discharge a two-phase mixture.

The output curve of dry steam wells MW-09 and 13 are almost flat within the tested WHP range, with rates only gently increasing when WHP is reduced. Flat output curves suggest strong incremental pressure drops for limited rate increments, as occurring when flowing conditions are close to chocking. Combined wellbore and reservoir simulation at a well sector scale for MW-09, calibrated to reproduce the output curve, showed that the flat curve is due to two distinct factors: i) the down-hole drawdown which is not linear as function of rate but is characterized by additional losses proportional to the square of mass rate; ii) the discharge conditions approaching choking at wellhead for WHP lower than 20-30 bara. When choked flow conditions are approached (speed

close to that of sound at local conditions) marginal increments of rate are obtained by further opening the well.The numerical simulations allowed also to estimate a possible increment of production rate for a well with reservoir conditions similar to that encountered by MW-09, but completed with a larger production CSG of 13 3/8 “, of about 30%.

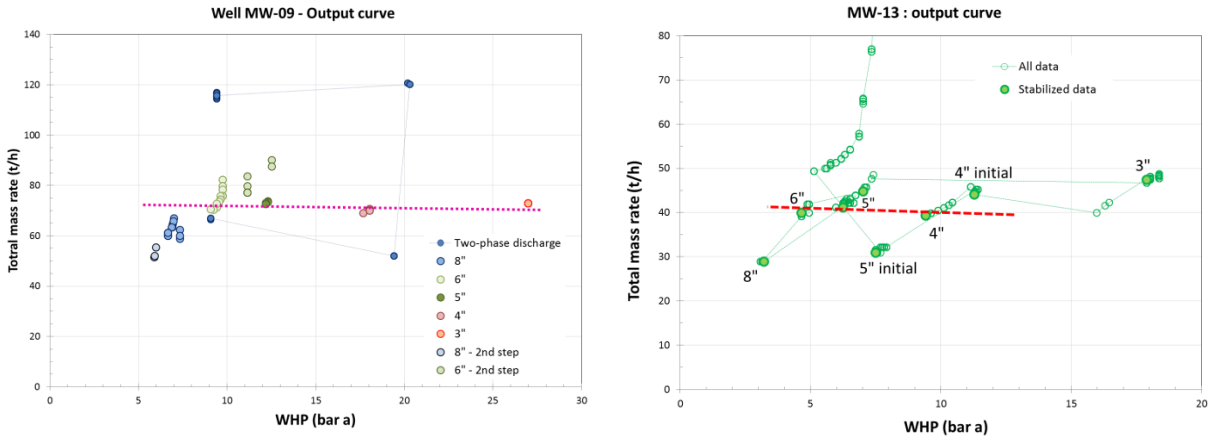


Figure 9: Output curves of wells MW-09 (left) andMW-13 (right), both discharging dry steam.

3. CONCEPTUAL MODEL

The conceptual model of the geothermal field is the synthesis of all the information obtained by the analysis and interpretation of the available data, both from surface studies and from deep exploratory wells, and was used as the basis for the resource assessment and for the study of the reservoir behaviour under exploitation, as well as for the evaluation of the field potential and for the definition of the optimum development strategy.

The essential features of the Menengai reservoir can be summarized as follows:

a. **Heat Source:** All available elements point to the extremely positive setting of the Menengai area in terms of heat source, in consideration of: (i) the post-calderic, very recent age of the eruptions, witnessing the active nature of the magmatic chamber(s), still in a molten stage with temperatures in excess of 700°C; (ii) the acidic nature of the erupted products, reflecting phenomena of differentiation which are generally accompanied by an uprising of the magma to a depth lower than about 8km; (iii) the widespread distribution of the recent eruptive centres, suggesting the large volume of the magmatic chamber(s).

b. **Geological Setting:** The permeability distribution within the Menengai geothermal system is attributable to two specific elements, namely the type of hydrothermal alteration and the degree of tectonic stresses which affected the geological formations. The propylitic zone, reflecting high temperatures and competent nature of the rocks, exhibits a dome-shaped configuration, with the top located in correspondence of a W-E oriented belt extending between MW-07 to the west and MW-03 to the east. With reference to the degree of tectonic stresses, it is observed that an intense neo-tectonic activity has taken place in the interior of the caldera. Within this general structural pattern, two major features have been identified, corresponding to two faults running NNW-SSE and N.7W-S.7E, which delimit a block of 4 to 6km wide, which is likely to be associated with a fracture density higher than average.

c. **Reservoir Geometry:** Two distinct geothermal reservoirs, hereinafter called shallow and deep reservoir, have been recognized.

The **top of the shallow reservoir** occurs at an elevation between 900 and 1300 m.a.s.l. (except in well MW-02, where it is not recognizable), corresponding to a depth bgl of 700-1100m and being expressed in the temperature profiles by a short stretch of iso-temperature indicative of a convective cycle. Such depth approximately coincides with the start of the important circulation losses registered in the wells of the central part of the field below the cap-rock and, in terms of alteration mineralogy, with the top of the secondary quartz zone. The **bottom of the shallow reservoir** is accordingly inferred to occur at an elevation between 600 and 1000 m.a.s.l.

Evidences for the existence of a shallow reservoir have been recognized in all the wells drilled to date except for MW-02. This reservoir is therefore deemed to extend throughout most of the sector investigated by drilling, being probably delimited to the west and east by the two major structures running N.7W-S.7E and NNW-SSE, to the north by a line between wells MW-02 and MW-11 and to the south by a line just south of MW-5A. These boundaries would indicate an **areal extent of the shallow reservoir** of approximately 20km^2.

The **top of the deep reservoir** exhibits a pronounced dome-shaped configuration, with the upper sector, at an elevation of 600-900 m.a.s.l., extending in a W-E direction between MW-01 and MW-04/MW-12 and in a N-S direction between MW-08 and MW-10/MW-12. Beyond these points, a sharp drop appears to take place in all directions (see wells MW-5A, MW-11, MW-14, MW-15 and MW-17). The above described configuration is similar to that of the top of the epidote, except for the larger W-E continuation of the latter parameter, which extends between MW-07 and MW-03. The **bottom of the deep reservoir**, expressed by the start of the conductive regime which may reflect impervious conditions of the rocks, is found at an elevation in the range of 0/-200 m.a.s.l. with local uprising, indicating an average thickness of the deep reservoir of 600-1,000m in the

central sector, dropping to <500m in the peripheral zone.The Menengai geothermal field resources have been classified into three distinct categories (see Figure 10):

- **Developed Area**: it corresponds to the sector where all the present producing wells are concentrated, extending over a length of about 3km in a W-E direction and of about 2.5km in the N-S direction and covering a total surface of approximately 7km^2.
- **Development Area**: it encompasses a sector located to the SW of the former area, defined from the structural and micro-seismic monitoring data, covering a total surface of about 3km^2. The reservoir thickness in this sector is interpreted to be in the order of several hundred meters.
- **Expansion Area**: it exhibits an oval-shaped configuration, forming a sort of a halo around the above mentioned categories; it is on the whole characterized by wells where adequate temperature conditions have been encountered, not accompanied by favourable hydrogeological conditions (MW-11, MW-15 and MW-17). This potential resource covers accordingly a surface of about 10km^2. The reservoir thickness within the expansion area is interpreted to be in the order of a few hundred meters.

The total surface of the geothermal resources, combining these three categories, can be accordingly estimated in about 20km^2.

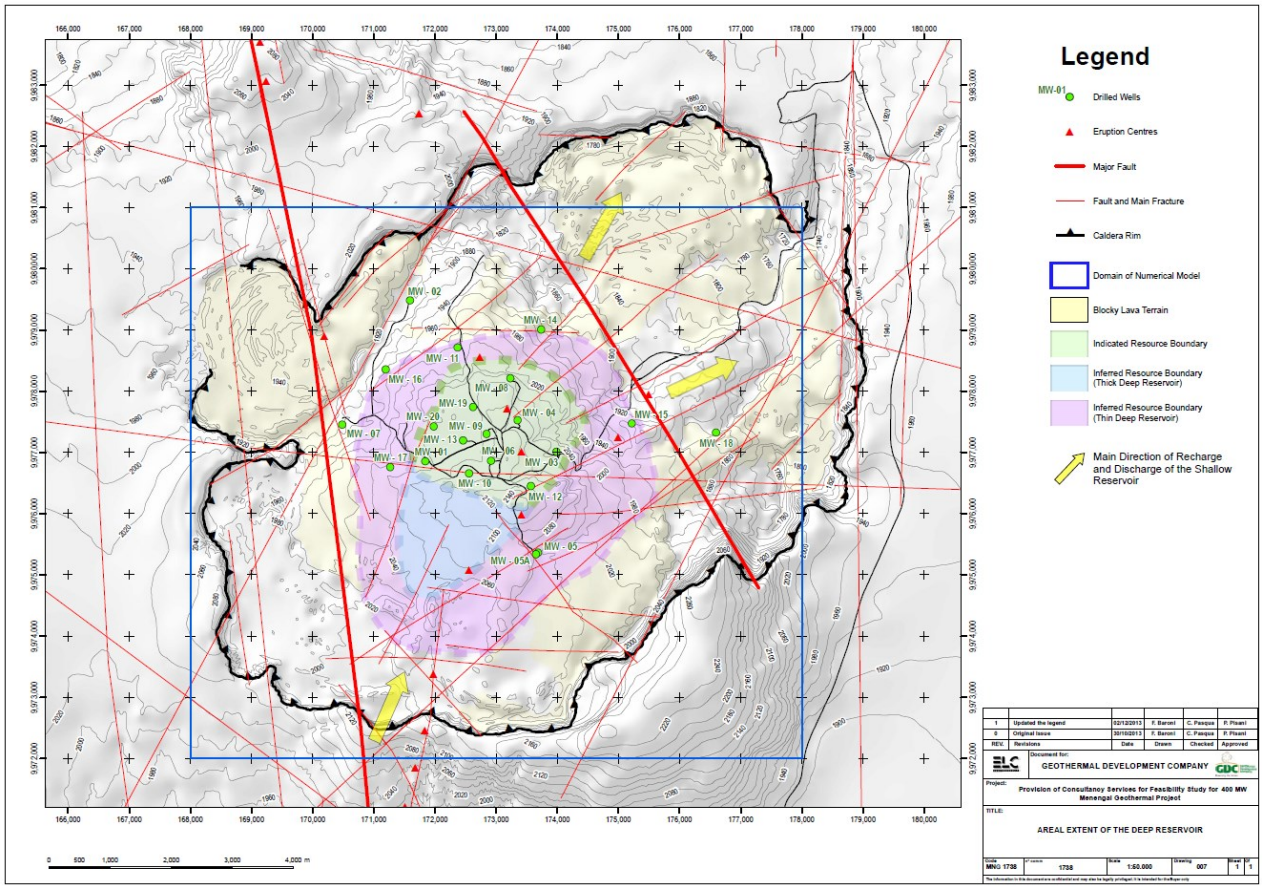


Figure 10: The figure 1 shows the main structural features of the Menengai caldera with the presumed deep reservoir extension (colored area), the presumed shallow reservoir recharge direction and the numerical model extension

d. Natural Fluids Flow Pattern: Due to a lack of determination of the isotopic content in the fluids of the deep wells, no direct information is available on the nature of the main recharge of the **deep reservoir**. Possibly such recharge takes place along the borders of the caldera, associated with the presence of major structures, which may favour the deep infiltration of meteoric water, with minor contribution from the magmatic system in the form of steam and gas transfer.

Upon getting in the proximity of the heat source corresponding to the active and rather shallow magmatic chamber, waters heat up and start to rise, following deep seated faults and crossing the whole sequence of geological formations (from Tertiary to recent times). In the course of their upraise the hot fluids tend to boil and to expand laterally along horizons associated with widespread fracturing.

The main upflow zone is situated in the central part of the Developed Area, in correspondence of the sector where the magmatic chamber forms a plume-like structure, getting closer to the surface. The two major faults running NNW-SSE and N.7W-S.7E seem to constitute a hydrogeological barrier to the eastern and western expansion of these fluids. No important escapes from the deep reservoir to the surface have been identified. Its areal configuration, suggests that the main outflow takes place along this W-E axis, possibly reflected by the geoelectrical anomaly recognized to the west of the caldera rim.

The recharge of the **shallow aquifer** appears to take place from the SSW of the sector under development. The fluids, upon getting above the deep reservoir, tend to heat up mostly as a result of conductive heat transfer and to reach their maximum temperature in coincidence with the main upflow zone of the deep reservoir. The main outflow of the shallow aquifer is likely to take place in an E to NE direction, moving then along a preferential N-S trend upon reaching the Solai Graben.

4. 3D NATURAL STATE MODEL

4.1 Numerical Model Approach

For the simulation of the natural state and exploitation scenarios a 3D model has been built using the TOUGH2 V.2.0 (Pruess et al., 1999) numerical reservoir simulator managed using Petrasim V.5.2 pre- and post-processing software package. Among the Equation of State (EOS) modules available within TOUGH2 V.2.0, considering the non-negligible NCG content in Menengai field (represented mainly by CO_2), the EOS2 module for mixtures of water and CO_2 was employed.

Considering the 3D geometry of Menengai prospect and its relevant features, an unstructured Voronoi grid approach was chosen, with upper grid layers following the DTM (digital terrain model) elevations and the reconstructed top and bottom of shallow and deep reservoirs. Petrasim allows as a first step to build a model at a conceptual level by defining the model geometry, layering, internal regions, boundary and initial conditions, sink and sources and petrophysical properties distribution, and in a second step to build the discretization grid. As far as the construction of Menengai numerical model is concerned, it has been performed according to the following steps:

- ✓ Starting from the conceptual model of the prospect, the area and the thickness to be modelled have been chosen.
- ✓ Layering at the conceptual level has been defined.
- ✓ Internal boundaries have been added, including the two main faults, and the deep and shallow reservoirs structure.
- ✓ Rock types and properties have been defined and their distribution within the modeled domain assigned according to the results of well logging and testing data.
- ✓ Initial and boundary conditions were assigned, including the location of inflow and lateral outflow zones of the shallow reservoir, and the upflow in the deep reservoir.

A series of simulations have been performed trying to obtain a stable steady-state with pressure and temperature distributions reproducing those observed in drilled wells. During this iterative process, main applied changes were relative to the inflow of the shallow reservoir, the temperature at the model bottom beneath the deep reservoir, the permeability of rock domains and to the features of the upflow recharging the deep reservoir.

4.1 Numerical Model Features

The numerical model covers an area of 8.715 × 8.8 km = 76,692 km^2, from 168643 to 177358 E, and from 9972100 to 9980900 N. The model reaches an elevation of 2268 m.a.s.l., which is the DTM maximum elevation. The bottom of the model was set to -1300 m.a.s.l. An unstructured grid is chosen according to the IFDM (Integral Finite Difference Model) spatial discretization approach on the horizontal plane with 1,398 elements per grid layer (Figure 11). For the construction of the Voronoi grid the settings were: a maximum element area of 2E6 m^2; a maximum area of 1400 m^2 for refinement elements; a minimum refinement angle of 30.2°. On the vertical direction 24 layers were used, for a total of 33,552 grid elements. Grid spacing and model dimensions have been chosen to properly cover the Menengai prospect surface, avoiding at the same time too many grid elements that would compromise simulation speed. The reservoir is limited by the faults on the Eastern and Western sides, but the model domain extends outside these faults. The deep reservoir extends down to a depth of -300 m.a.s.l., with a profile obtained from wells log data. The hot intrusion located below is taken as the bottom thermal boundary, set at 330°C, according to temperature measurements showing a conductive heat flow section at the reservoir bottom.

The deep reservoir also have a ‘rim’ with the same porosity value but lower permeability, that is not directly heated up by the bottom hot intrusion and which might represent the lower temperature section (at nearly 270°C) of the reservoir evidenced by the geochemical findings, as well as the extension of the two-phase zone evidenced by the Vp/Vs distribution inferred by the seismic investigations (Simiyu, 2009).

Major layers in the conceptual Petrasim model, to be distinguished from grid layers, are (from top to bottom):

Petrasim layers	Description
Top	A 300 m thick layer used to assign top thermal boundary conditions, followed by host rock down to the shallow reservoir
ShallRes	The shallow reservoir
Bulk	The host-rock
DeepRes	The deep reservoir, outcropping from the bottom, divided in two units.
Bottom	The bottom layer, used to set the thermal bottom conditions and containing the ‘hot intrusion’.

The top boundary layer is at fixed conditions of 85 C according to borehole and steam vents temperatures. The bottom boundary has a temperature of 300°C, and a hot intrusion (i.e. elements from the base to the bottom of deep reservoir in the central prospect area) set at 330°C.

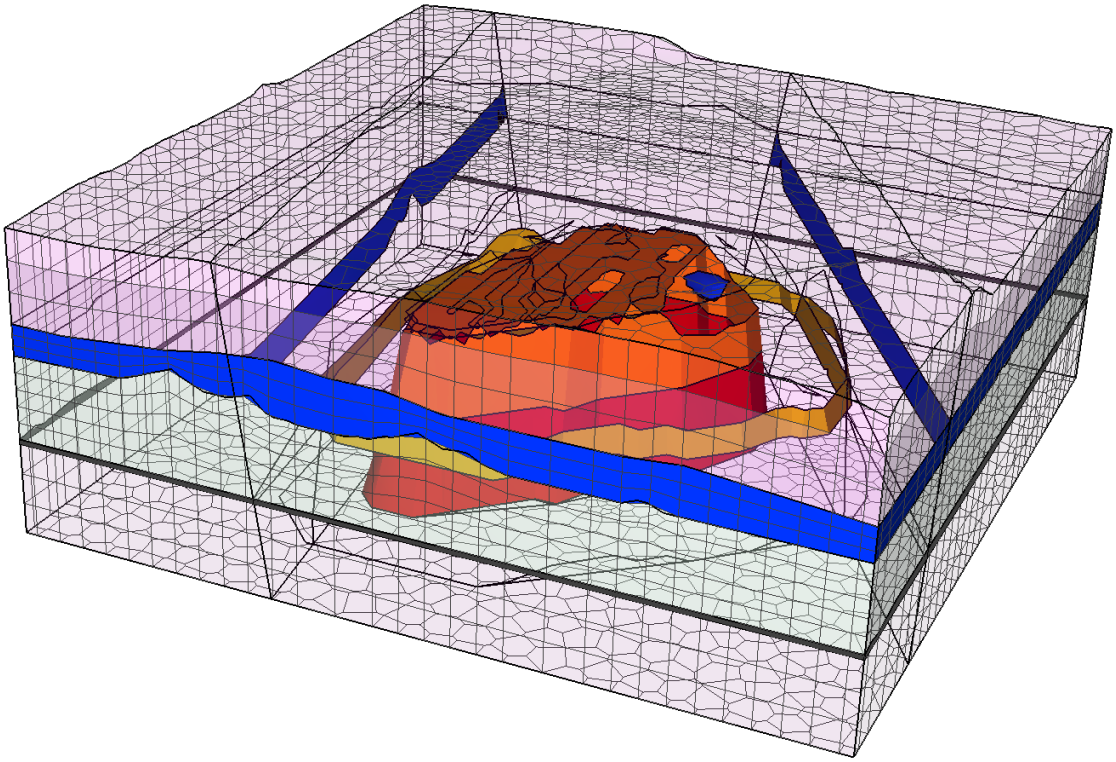


Figure 11: Menengai model structure, with the Shallow Reservoir in blue, the deep reservoirin orange, the hot intrusion in red and the external part of the deep reservoirin dark-yellow.

According to the conceptual model findings, the deep reservoir is surrounded by very low permeability rocks, and is recharged by an up-flow of a 320°C fluid with a CO_2 of 5% by weight. The shallow reservoir has a salinity of 12,000mg/kg, with an inflow roughly corresponding to the rainfall inflow and an outflow to the W and N controlled by a constant pressure boundary set at 70bar. While any possible effort has been done to incorporate the major features of conceptual model developed for the Menengai prospect, several assumptions were needed to develop the numerical natural state model. The calibration process allows reducing the uncertainties related to some of these assumptions. For others, the uncertainty remains high, in particular outside the drilled area so far. In Table 1 the properties of the main rock units assigned to the final 3D numerical model are reported.

Domain	Description	k_x, k_y(m^2)	k_z(m^2)	φ	c_R(kJ/kg)	λ_R(W/(m °C)	ρ_R(kg/m^3)
TOP	Top structure	1.E-22	1.E-22	0.02	1400	2.0	2600
SHALL	Shallow reservoir	2.E-14	2.E-15	0.06	1400	2.0	2600
BULK	Host Rock	1.E-22	1.E-22	0.02	1400	2.0	2600
RES	Deep Res.central part	2.E-14	1.2E-14	0.06	1400	2.0	2600
RESEX	DeepRes.external part	1.E-14	1.2E-15	0.06	1400	2.0	2600
BOTHH	Botton hot intrusion	1.E-22	1.E-22	0.02	1.E+50	2.0	2600

Table 1: Main properties for rock domains used in the final 3D natural state model. The huge rock specific heat assigned to the bottom intrusion is used to maintain a constant temperature throughout the simulation.

4.1 Model Results

After model set-up, the numerical model was run for long simulation times until a reasonable steady-state was reached, with stable thermodynamic conditions and fluid flow distribution through the system. The results of the 3D steady state were then compared with measured temperature profiles to check the reliability. Figure 12 reports the comparison between simulated and measured temperature in wells MW-01, MW-03, MW-06, MW-08, MW-09, and MW-12.

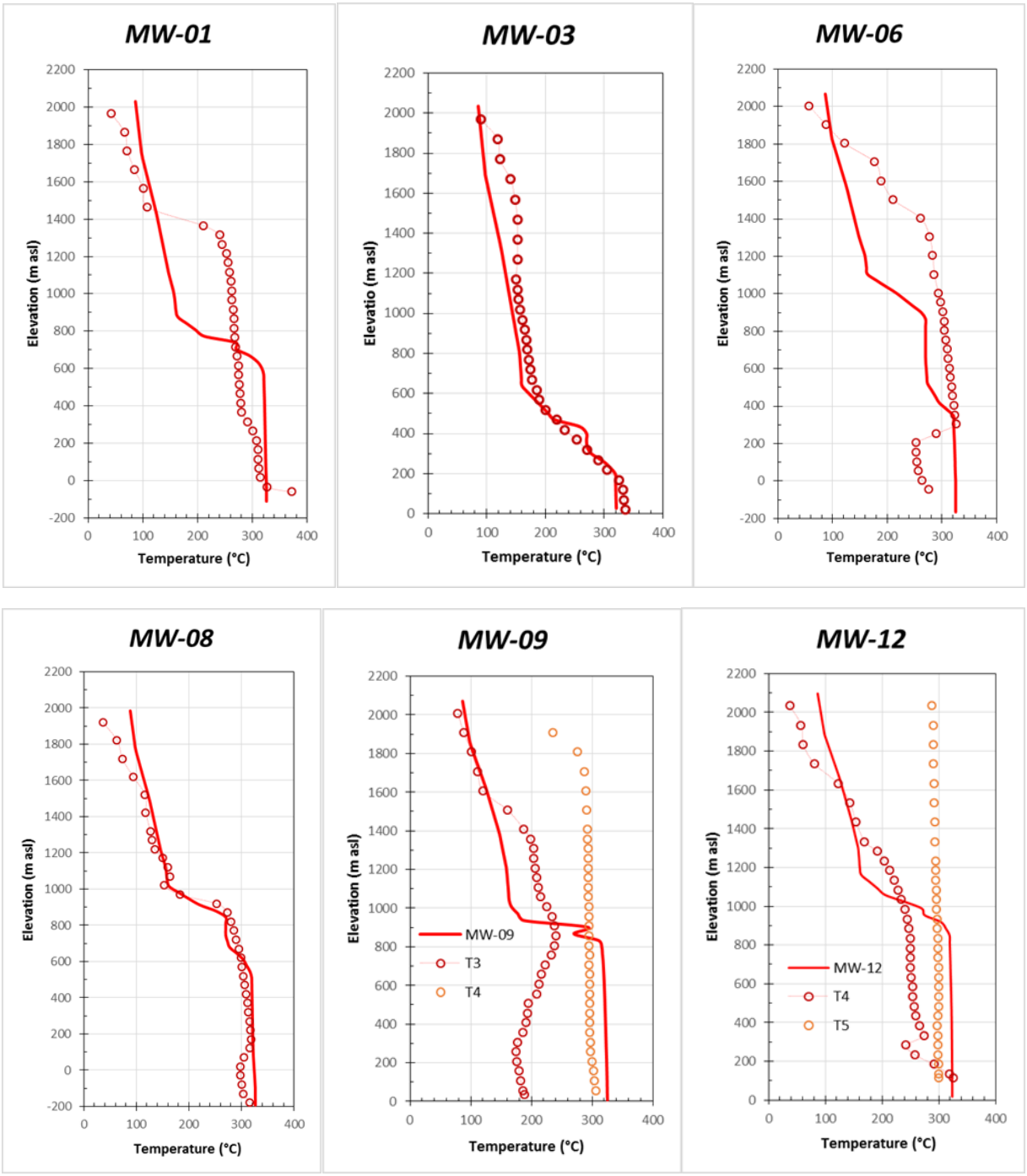


Figure 12: Simulated temperature profiles of selected wells (continuous lines) compared to measured profiles (circles).

Simulated and measured temperature profiles are in reasonable agreement, considering that stable conditions were difficult to be observed in most of drilled wells because of inter-zonal flows and boiling process within the wellbores. The comparison suggests that the simulated natural state is able to reproduce both the deep and shallow reservoir temperature distributions, but is not accurate in the top most part, mostly due to the thick layer used and to the shallow ground water aquifers crossed by the wells but not included in the model. Wells MW-06, MW-09, and MW-13 show a similar profile, being located in the main structure of the deep-reservoir not far from each other. MW-06 shows a clear feed at nearly 300 m.a.s.l. that supplies dry steam and generates an upward heating of the borehole.

The simulated natural state is presented using the distribution of main thermodynamic parameters along vertical and horizontal sections. Liquid dominated and two-phase vapor dominated conditions are obtained for the shallow and deep reservoirs, respectively. Figure 13 shows (from a S view) the temperature distribution in a E-W section intermediate to well MW-13, 9, and 3 with the major up-flow on the left (western) side of the deep reservoir and a minor upflow in the other deep reservoir culmination. The N-S section of the deep reservoir with temperature distribution and total fluid flow, cut across well MW-09, is shown in Figure 14, where we can recognize the two up-flows. This figure shows the relationship between the inner, hotter volume of the reservoir and its morphology. The deep reservoir outflow, mainly represented by the fluids escaping upwards into the shallow reservoir and feeding the fumarolic field, is evidenced by the total flow vector. The pressure in the deep reservoir follows the same behavior, as shown in Figure 17.

The simulated gas saturation distribution in Figure 15 shows that high values are present within the deep reservoir, whereas at its border the gas saturation is reduced to values as low as 0.2. Looking at the temperature distribution, the temperature rim at 270-300°C could be observed. Such results are not unexpected, since pressure distribution in the deep reservoir is along a water-CO_2 mixture boiling curve, and CO_2 is concentrated mainly at the top of deep reservoir due to boiling and condensation linked to a heat pipe process.

For having a complete picture of the deep reservoir conditions, in Figure 16 the distribution of CO_2 in the deep reservoir is shown together with NCG flow vectors, evidencing the NCG accumulation at the top of the deep reservoir. The NCG flows to the upper culmination in the area within wells MW-06 and 09 where the highest top of the reservoir is found, and the impact of deep fluid on the shallow reservoir is more evident. Due to the consideration of fluid outflow from the deep reservoir towards the surface, an outlet for the deep reservoir is located in the structural top close to well MW-09, and controlled with a constant outlet pressure. It is evident the lack of a uniform pressure gradient in the whole structure. In particular the deep reservoir shows a pressure lower than expected. Anyway, in particular in Figure 17, it is evident that the shallow and deep reservoirs are very close, and could have some hydraulic connection.

The obtained natural state is thus able to take into account the main features of the conceptual model, and through the guessed boundary conditions it allows to obtain pressure and temperature distributions close to that provided by well logging, despite non-well stabilized conditions were present down-hole in most of the drilled wells. The obtained natural state was then used to model production and reinjection scenarios not discussed in the present work. These further modeling activities pointed out that some parameters are still poorly constrained, like the effective reservoir extension in the unexplored area.

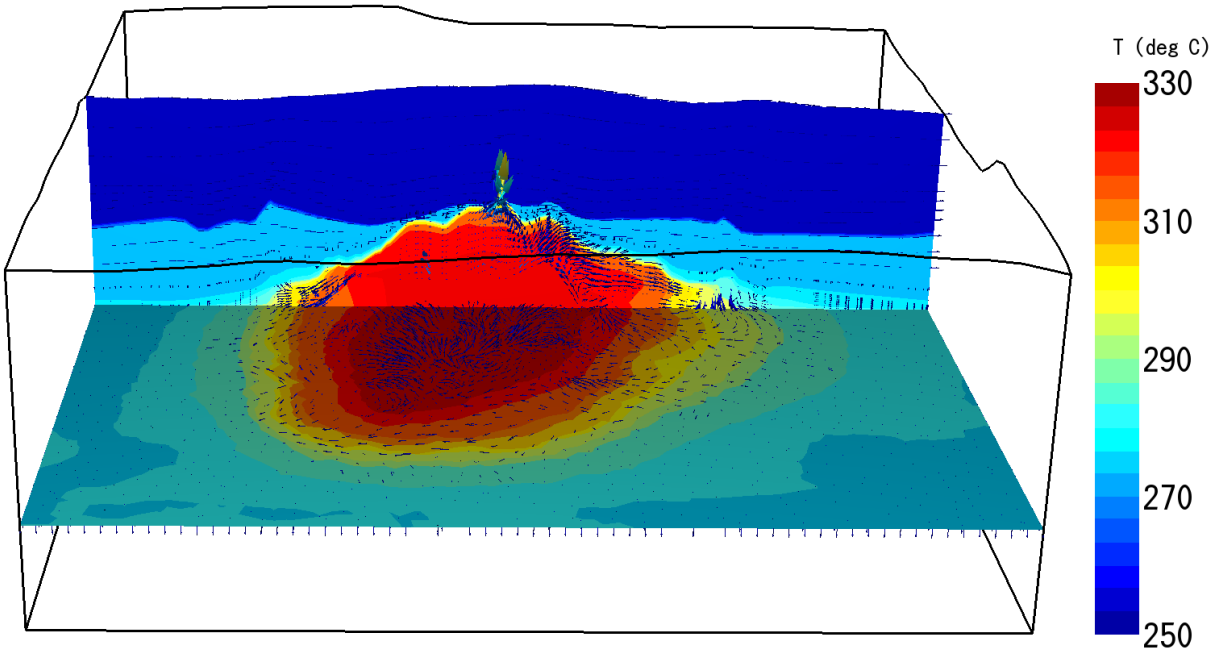


Figure 13: Reservoir temperature distribution with total fluid flow vectors along a E-W section at 9977400 m and a N horizontal section at -300 m.a.s.l.

5. CONCLUSIONS

The Menengai caldera is an elliptical depression located near Nakuru, Kenya's Rift Valley, with minor and major axes measuring about 8 and 12 km, respectively. It was recognized as a promising geothermal prospect among the many existing along the Rift Valley in Kenya. Geophysical investigations (micro-seismic monitoring, gravity and MT surveys), geological surveys, geochemical surveys (fumaroles sampling, soil gas surveys) and a soil temperature survey allowed GDC to locate the first exploratory well MW-01 which intercepted a deep reservoir with temperatures exceeding 300°C, found beneath a shallower liquid-dominated reservoir at temperatures in the range of 190-200°C. Following this success, an exploratory and development campaign provided the drilling of 20 deep wells by December 2013 aimed at characterizing the deep reservoir properties, delineate the field extension and provide additional steam for power development. The review of available data allowed to build a conceptual model of the Menengai geothermal system which is characterized by the presence of a liquid dominated shallow reservoir at temperatures ranging between 130 and 210°C, which overlays a deeper high temperature, two-phase vapor dominated reservoir with temperatures reaching 330°C. A conceptual model of the entire system was developed incorporating surface exploration surveys and the findings derived from drilling, logging and testing of geothermal wells.

The conceptual model, integrated with production testing results, was used to build a 3D numerical model of the geothermal system in order to simulate its natural state, check the consistency of acquired data, and set up the tool for the subsequent modeling of exploitation scenarios. The numerical model was built with the TOUGH2 reservoir simulator using the EOS2 thermodynamic module. The model setup and numerical simulations were supported by the Petrasim 5.2 graphical interface. The modeling of the natural state was intended to check the consistency of the conceptual model, give a better picture of the reservoir thermodynamic conditions and constrain the mass and heat flows through the system. The model was run to steady-state conditions, and calibrated

against data obtained from geochemical investigations, well pressure and temperature profiles recorded under warm-up and flowing conditions, as well as available production test results. The 3D natural state reasonably reproduces the liquid dominated shallow reservoir just on top of the deeper, two-phase vapor dominated high temperature reservoir which feeds the dry steam wells drilled in the central area of the prospect. The deep reservoir is recharged by the up-flow of a high temperature mixture of steam and CO_2. The latter accumulates at the culminations of the deep reservoir due to the boiling and condensation processes associated to the heat pipe mechanism supported by the strong heat flow. The gas phase saturation declines, moving from the central vapor-dominated area towards the periphery of the deep reservoir, where the aqueous phase becomes strongly mobile. The thermodynamic conditions and rock properties of the lateral extension of the deep reservoir are poorly constrained by present drilled wells and need to be better characterized in the future, as they are fundamental for a reliable assessment of overall prospect potential.

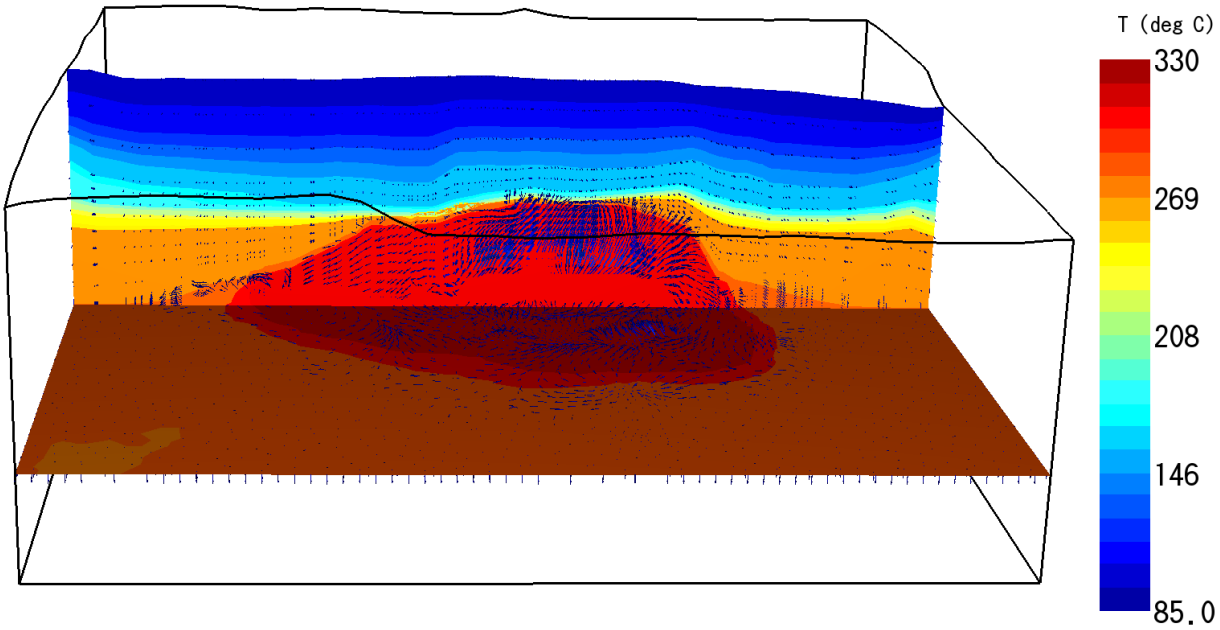


Figure 14: Reservoir temperature distribution with total fluid flow vectors along a N-S section at 172600 mE and horizontal section at -300 m asl

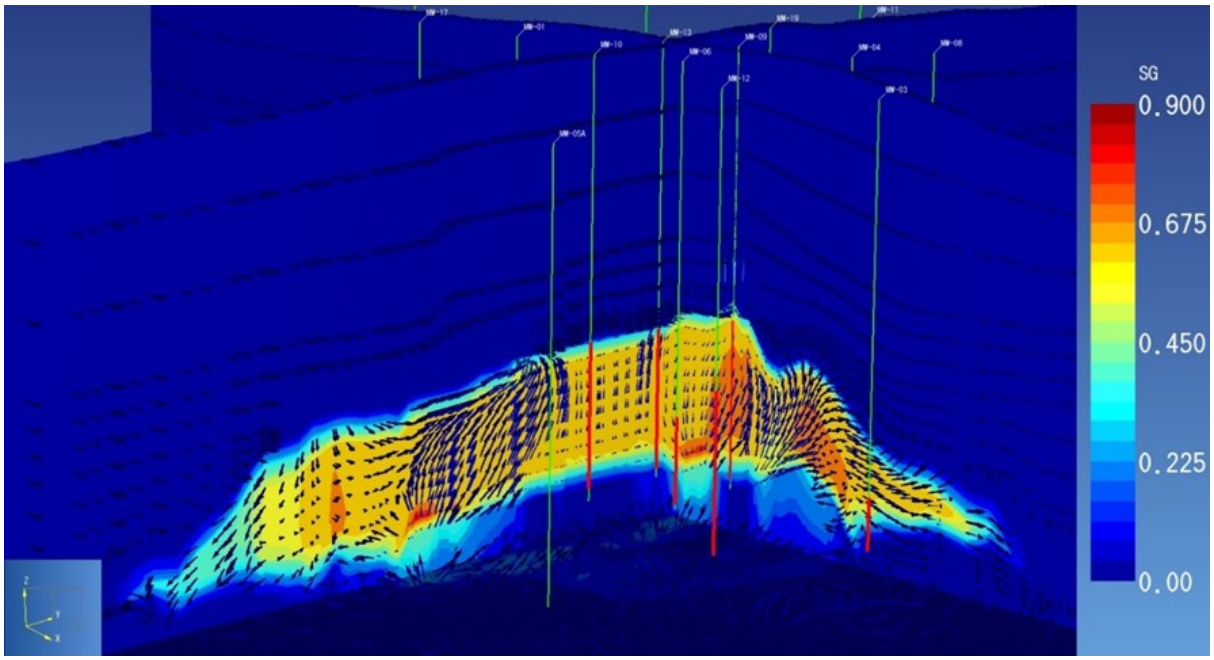


Figure 15: Gas phase saturation distribution within the deep reservoir with fluid flow vectors. Horizontal section at -200 m.a.s.l. and vertical slices at 1.724E5 mE and 9.9773E6 mN, viewpoint from SE.

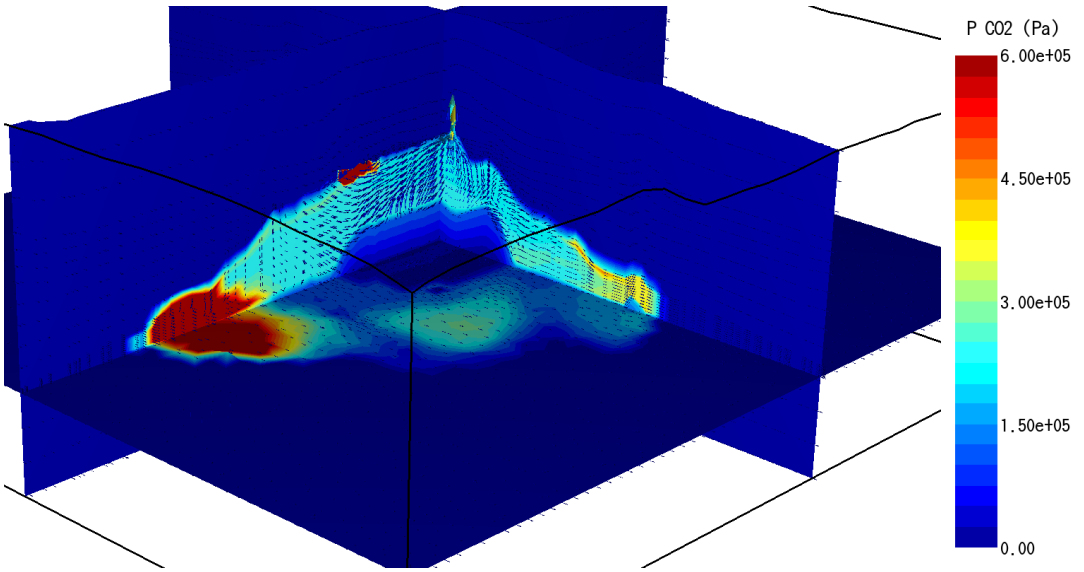


Figure 16: CO_2 partial pressure distribution with NCG mass flow vectors along an E-W section at 9977400 mN, a N-S section at 172700 mE, and a horizontal section at -300 m.a.s.l.

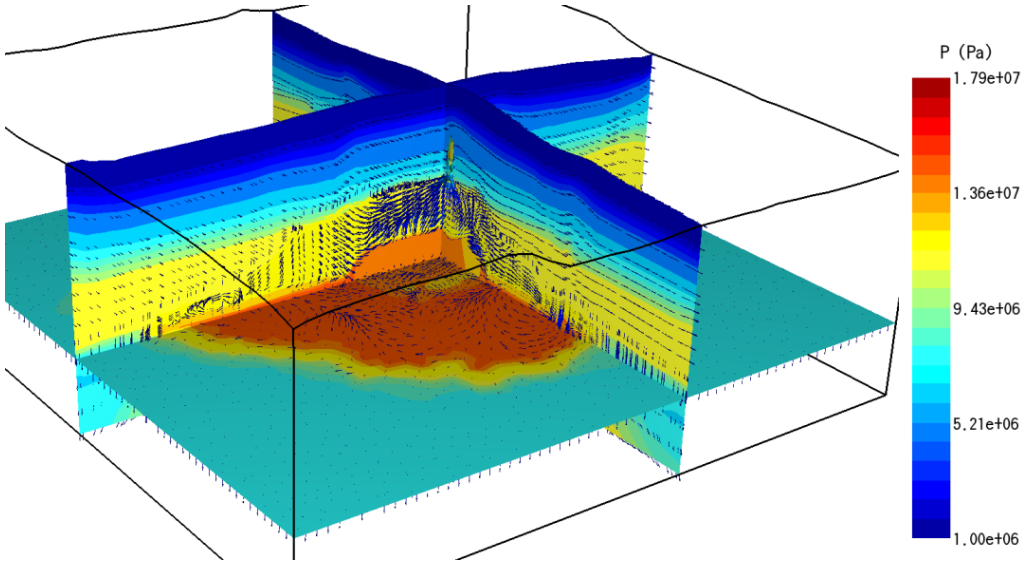


Figure 17: Reservoir pressure distribution with total fluid flow vectors along a E-W section at 9977400 mN, a N-S section at 172700 mE, and a horizontal section at -300 m.a.s.l.

REFERENCES

James C.R.: Steam-water critical flow through pipes, Proc. Institute of Mech. Eng., 176 (26), (1962), 741.

James C.R.:Factors controlling borehole performance, U.N. symposium on the Dev, and Util. of Geoth. Resources, Pisa. Vol.2, Part. 2, (1970), 1502-1515.

O'Sullivan M.J., Bodvarsson G.S., Pruess K., Blakeley M.R.: Fluid and Heat Flow in Gas-Rich Geothermal Reservoirs, *SPE Journal*, **25** (2), (1985), 215-226.

Pruess K., Oldenburg C.M., Moridis G.J.: TOUGH2 User's Guide, Version 2.0, Report LBNL-43134 (1999).

Simiyu S.M.: Application of micro-seismic methods to geothermal exploration: examples from the Kenya Rift, Short Course IV on Exploration for Geothermal Resources, UNU-GTP, KenGen and GDC, Lake Naivasha, Kenya, November 1-22, 2009.